
Article:
Goodall, A.D. orcid.org/0000-0002-4773-0321, Chechik, L. orcid.org/0000-0002-7626-2694, Livera, F. orcid.org/0000-0001-6154-0594 et al. (1 more author) (2024) Importance of surface roughness on the magnetic properties of additively manufactured FeSi thin walls. Acta Materialia, 263. 119501. ISSN 1359-6454

https://doi.org/10.1016/j.actamat.2023.119501

Acta Materialia 263 (2024) 119501

Contents lists available at ScienceDirect

Acta Materialia

journal homepage: www.elsevier.com/locate/actamat

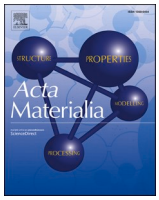

Full length article

Importance of surface roughness on the magnetic properties of additively manufactured FeSi thin walls

Alexander D. Goodall [a,*], Lova Chechik [a], Frances Livera [a], Iain Todd [a]

[a] Department of Materials Science and Engineering, University of Sheffield, Sheffield, UK

ARTICLE INFO

Keywords:
Laser powder bed fusion
Soft-magnetic material
FeSi: Anisotropy
Surface roughness

ABSTRACT

Thin-walled structures are being used in soft magnetic components manufactured by additive manufacturing to limit eddy current losses in AC machines. Fe-6.5wt %Si has been shown to be a promising material in such components, however most characterisation has taken place using thicker bulk material. Thermal conditions and microstructure have been shown to differ within thin-walled structures, hence magnetic properties may also differ. This study characterises the magnetic properties of thin-walled structures, showing that the ⟨001⟩ texture usually apparent in laser powder-bed fusion does not persist in thin-walled samples built at an angle to the build platform. Surface roughness (S_a) is shown to increase with build angle from 28 μm when perpendicular to the build platform, to 80 μm when parallel, causing a deterioration in magnetic properties such as susceptibility which is reduced by up to 25 %. Improvements in magnetic properties are demonstrated for samples with lower surface roughness due to improved laser parameters, with even larger improvements available when using polishing as a post-process finishing operation which was shown to improve susceptibility by over 10 %. This study enables the designers of soft magnetic components made by additive manufacturing, the freedom to design magnetic flux paths at any angle in the build chamber and gives surface roughness as a key parameter to improve magnetic properties.

1. Introduction

Research interest in additive manufacturing (AM) of soft-magnetic materials started when Zhang et al. processed permalloy (Fe-30 % wtNi) [1], and has greatly increased in the last decade with many authors contributing to the field [2–4] with studies focusing on the three most common soft-magnetic alloys of FeSi [5–7], FeCo [8–10] and FeNi [11–13]. Of these materials, FeSi is the most heavily used commercially with a wide variety of applications. AM has been used to demonstrate manufacturing of transformers [14,15], electric machine stator cores, and rotors [5,16]. Throughout these applications, all of which operate using AC currents and magnetic fields, thin walled structures are deployed to reduce eddy currents and their associated joule heating losses [6,7,17], mimicking the behaviour of electrical steel laminations whereby eddy currents are confined to smaller cross-sectional areas normal to the magnetic flux. Although the material is normally used in a thin wall (<2 mm) structure, the properties have always been measured with cross-sectional dimensions above 4 mm [6,7,18] for ease of handling and characterisation, and to abide by standards for characterisation such as BS 60,404 [19].

Heat transfer in thin walls has been shown to behave differently than bulk material (>4 mm thickness) during AM [20], yielding differing microstructure based upon the geometry. Assuming this to be the case in AM of soft-magnetic materials, the microstructure and hence magnetic properties of these thin wall structures cannot be directly implied from measurements of the bulk material. Further to this, authors often refer to an improved magnetic performance in the build direction of Fe-6.5wt % Si during l-PBF due to a strong ⟨001⟩ texture in this direction whilst avoiding the ⟨111⟩ direction [6,14,15,21,22]. This texture has only been demonstrated in thicker samples, generally with a cuboidal structure unlike those likely to be used in an electrical machine. There is no evidence yet to suggest that the properties are different in different build orientations, however one study does investigate rings built at different build orientations [23], but fails to draw conclusive differences between the samples. In low silicon (Fe-3wt %Si) electrical steel laminations, grain orientation is often used to obtain better properties by aligning a goss texture with the magnetic flux direction, supported by measurements on single crystal materials [24] and polycrystal steel sheets [25].

* Corresponding author.
E-mail address: adgoodall1@sheffield.ac.uk (A.D. Goodall).

https://doi.org/10.1016/j.actamat.2023.119501
Received 30 January 2023; Received in revised form 21 September 2023; Accepted 5 November 2023
Available online 6 November 2023

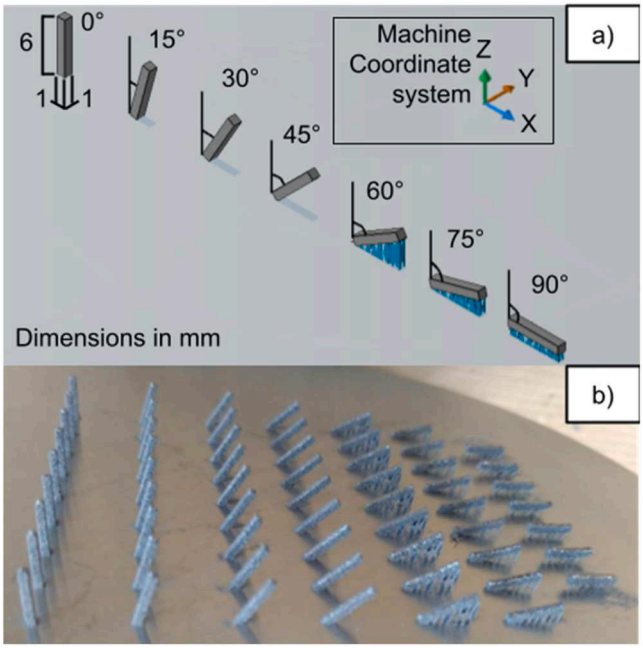

Fig. 1. Sample orientation, machine coordinate system and labelling nomenclature (a) with a photo of the samples in the as-built condition (b).

However high silicon electrical steel (Fe-6.5 wt %Si) has a magneto-crystalline anisotropy constant of $k_1 = 3.4 \times 10^4$ J/m^3, 20 % lower than Fe-3 wt %Si at $k_1 = 4.1 \times 10^4$ J/m^3 [26]. This means that at the higher silicon content of 6.5 %, there is less difference between the easy ⟨001⟩ and hard ⟨111⟩ axes of magnetisation. There is a need for further understanding of the magnetic properties of soft-magnetic materials processed by AM, especially thin-walled components. Without this understanding it will not be possible for electrical engineers to simulate electrical machine performance, or design improved machines using materials produced by AM.

This study will investigate the grain orientation and surface roughness of thin-walled samples built at a variety of angles within the build chamber, characterise texture using electron backscatter diffraction (EBSD), and magnetic properties using vibrating sample magnetometry (VSM). Samples built at a variety of angles to the build platform will be characterised for both magnetic properties and microstructure. The effect of surface roughness on magnetic properties in thin-walled structures will also be investigated, and optimised build parameters and post-processing attempted to improve performance.

2. Materials and methods

2.1. Sample processing

All samples in this study were manufactured from high silicon steel powder (Fe-6.5wt %Si) with a size range of 15 - 45 μm supplied by Höganäs, using an AconityMINI (Aconity3D GmbH) L-PBF system, equipped with a 200 W ytterbium doped continuous wavelength laser (wavelength 1074 nm) which has a spot size of 70 μm. All samples were built using a meander scan strategy with laser power 170 W, laser speed 670 mm/s, and a hatch spacing of 70 μm which was previously found to give above 99.5 % density in 5 × 5 × 5 mm cubes. The samples were processed with a variety of contour parameters, ranging from 0 to 2 contours with varying volumetric energy density specified by using a full factor design of experiments, with 4 levels of laser speed between 500 - 1100 mm/s, and 4 levels of laser power between 130 - 190 W resulting in a volumetric energy density of 56 - 181 J/mm^3. Unless otherwise specified samples were built without contours. Sample orientation in the build chamber was varied from an angle of 0° to the machine Z axis, in increments of 15° about the Y axis until 90°, as displayed in Fig. 1, which also highlights machine coordinates. The Z axis is also referred to as the build direction. Samples were removed manually due to their size, by applying a small mechanical force at the base of the sample where it joins the stainless steel baseplate. Samples above 45° were built using supports.

2.2. Sample preparation, optical microscopy and EBSD

Samples were prepared for both optical microscopy and EBSD by hot mounting then grinding and polishing. Hot mounting in Bakelite was completed using a Simplimet 1000 from Buehler. Grinding and polishing was completed using a Struers Tegramin 20, first with grinding papers of P1200 and P2400, followed by 9 μm, 1 μm, and 0.25 μm diamond suspensions and a final polishing step using 0.05 μm MasterPolish, all supplied by Buehler. Polishing of samples for improved magnetic performance used only P1200 and P2400 grit paper grinding to improve the surface roughness by hand until an even finish was obtained. The surface roughness was re-measured using methodology as per Section 2.5.

Optical microscopy was undertaken using an Olympus BX51 microscope paired with Clemex Vision PE system. All optical micrographs were taken in the XZ plane of the machine coordinate system. Density analysis was completed using the areal method by thresholding the image in ImageJ.

Samples remained in Bakelite for EBSD analysis. EBSD analysis was conducted using a 7900F field emission gun (FEG) scanning electron microscope (SEM) manufactured by JEOL, fitted with an Oxford instruments symmetry EBSD detector. The accelerating voltage used was 20 kV with a step size of 1 μm. The Bakelite was reduced in size using hand tools, then mounted onto the SEM stub using silver suspension. The software used to capture EBSD data was AZtec by Oxford Instruments, indexing Fe-6.5wt %Si by using the library parameters for α-iron (BCC). Only a single phase was detected with an index rate above 98 %. Multiple frames were captured and aligned in the software before exporting to .crc format.

Analysis of the data was completed using MTEX toolbox plugin for MATLAB R 2020a. First the data was aligned to the machine coordinate system in order to create consistency within the data set. 10° was used to identify high angle grain boundaries and grain orientations were calculated. All orientation maps in this study are viewed on the XY plane. As per optical microscopy, all EBSD maps were captured on the machine XZ plane. Grain size (GS) was averaged using this data taking the arithmetic mean of the grains identified in MTEX. Weighted grain size (WGS) was calculated using Eq. (1), where n is the total number of grains.

$$WGS = \frac{\sum_{i=1}^{n} GS^2}{\sum_{i=1}^{n} GS} \quad (1)$$

Magnetic polarisation was calculated as a function of angle using the methodology from MTEX [27], based upon literature from several authors [28–31]. This methodology calculates the value of the magnetic anisotropy constant k1 (Eq. (2)) and magnetic saturation J_s (Eq. (3)) based upon the composition of the FeSi alloy [26]. Following this, the magnetic anisotropy energy, E_a, is calculated based on the orientations of the grains within the EBSD map (Eq. (7)) and averaged into angled bins between −90° and +90° from the samples long edge. Then J_{50} is calculated based upon the mean magnetic anisotropy energies (Eq. (8)). Al content is 0 wt % for all samples in this study.

$$K_1 = 4.77 - 0.21256 \times Si\ content\ (wt\%) - 0.03816 \times Al\ content\ (wt\%) \quad (2)$$

$$J_s = 2.162 - 0.043 \times Si\ content\ (wt\%) - 0.0625 \times Al\ content\ (wt\%) \quad (3)$$

$$Cos_{[100]} = \cos(angle\ between\ Miller\ [100]\ and\ grain\ [100]) \quad (4)$$

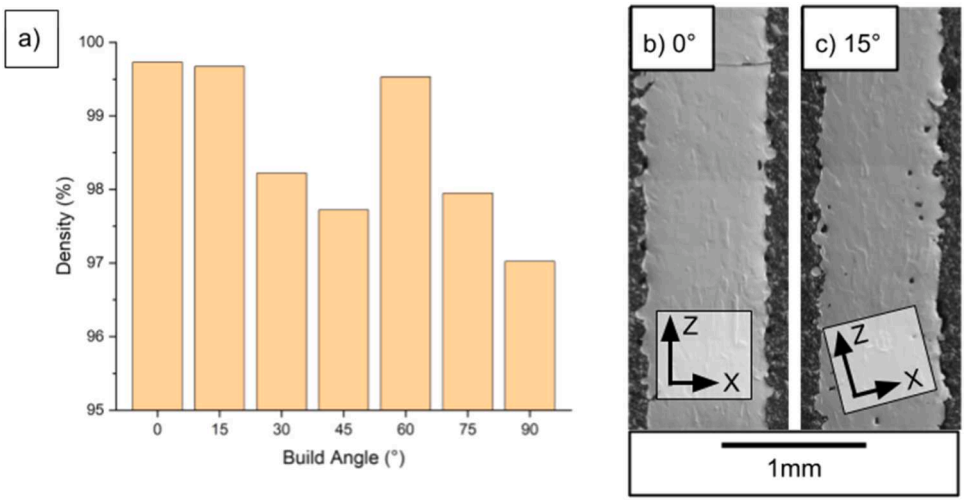

Fig. 2. Density vs build angle (a) with micrographs of 0° sample (b) and 15° sample (c) showing high density with a small amount of porosity present.

$$Cos_{[010]} = \cos(angle\ between\ Miller\ [010]\ and\ grain\ [100]) \quad (5)$$

$$Cos_{[001]} = \cos(angle\ between\ Miller\ [001]\ and\ grain\ [100]) \quad (6)$$

$$E_a = K_1 \times \left(Cos^2_{[100]}.\ Cos^2_{[010]} + Cos^2_{[100]}.\ Cos^2_{[001]} + Cos^2_{[010]}.\ Cos^2_{[001]}\right) \quad (7)$$

$$J_{50} = J_s(1 - 0.19 \times average\ E_a) \quad (8)$$

2.3. Magnetic characterisation using VSM

Magnetic characterisation was completed using an MPMS 3 magnetometer from Quantum Design UK. Samples were mounted on a quartz rod using GE varnish with the long edge of the sample aligned parallel to the magnetisation direction. Sample offset was measured at a field of 1.5 kA/m and the sample was centred from this. All measurements were taken at 300 K in VSM mode. 6 quadrants of a MH loop (magnetic moment vs field) were measured to allow the sample to saturate before data was taken and avoid demagnetisation cycles, which went from a field of 0 kA/m, up to 1200 kA/m, returning back to −1200 kA/m before again going to 1200 kA/m and then back to 0 kA/m. Results reported are from the fifth quadrant giving the magnetisation during a field change of 0 kA/m to 1200 kA/m, which was previously found to saturate the sample fully. 100 measurements were taken between 0 - 1200 kA/m using the uniform spacing$^{0.5}$ function, which gives a finer field spacing in lower values and a coarser spacing at higher values. The sample was held stable at each field, where a VSM measurement of amplitude 1 mm, averaging time 2 s was taken. All MH data plotted in this study uses normalised magnetic moment of M/M_s, which will allow for direct comparison of the shape of the loops whilst avoiding the requirement to correct for any radial offset or shape effects. It is possible to normalise this data in such a way as the sample is a single phase material and therefore the saturation magnetisation depends only on the volume of material. Heat treatment may cause the introduction of B2 and D03 phases as the samples were furnace cooled, however should not impact on the saturation of the material [32]. To ensure this is correct, several samples were tested before and after heat treatment, and were found to have the same M_{sat} during VSM measures.

Normalised susceptibility is calculated by finding the gradient between measured points at 3 kA/m and 35 kA/m. This was then normalised to the 0° as-built sample to allow easier comparison between samples.

2.4. Heat treatment

Heat treatment of samples, unless otherwise specified, was completed at 1150 °C for 1 hr, with a heating rate of 5 °C/min and furnace cooling as reported by Garibaldi et al. [22]. This was undertaken in a tube furnace under argon. For other samples held for different durations, the samples were removed from the furnace sequentially with the furnace still on, meaning that furnace cooling was not possible. Hence, the samples were removed from the furnace, kept in the ceramic boat, and placed in an insulating ITM-Fibermax 72 (Schupp) blanket to simulate furnace cooling. Samples were still not fully cooled after over an hour from removal so this was judged to be an acceptable method.

2.5. Surface roughness measurements

Surface roughness measurements were carried out using an Alicona InfiniteFocusSL using the optical focus-variation technique. Objective magnification of 5x was used and an area of approximately 2 × 1 mm was measured for each sample. The surface arithmetic average roughness (S_a) was obtained from a smaller section of approximately 1 × 0.5 mm, to avoid including edges and corners in the measurement. Error was measured by repeating this measurement 5 times for each sample, then using the standard error calculation as per Eq. (9), where SE is standard error, σ is standard deviation and n is the number of samples, 5 for this study.

$$SE = \frac{\sigma}{\sqrt{n}} \quad (9)$$

3. Results

3.1. Effect of build angle on microstructure

FeSi built by AM has been reported to have a ⟨001⟩ texture in the build direction, Z [33]. To confirm if this ⟨001⟩ texture remains in the same direction, even when thin rods are built at an angle to the build direction, samples were built at 15° intervals from Z (0°) to horizontal in the build chamber in the X direction (90°). As the removal of heat from the sample may flow through the component, due to the powder bed acting as an insulator relative to the solidified component, it was prudent to confirm that the ⟨001⟩ texture remained with the machine co-ordinate system or with the sample co-ordinate system, if it persisted at all.

Fig. 2a shows the density of the samples as they move away from 0°, demonstrating near fully dense (>99.5 %) for the 0° sample, with some

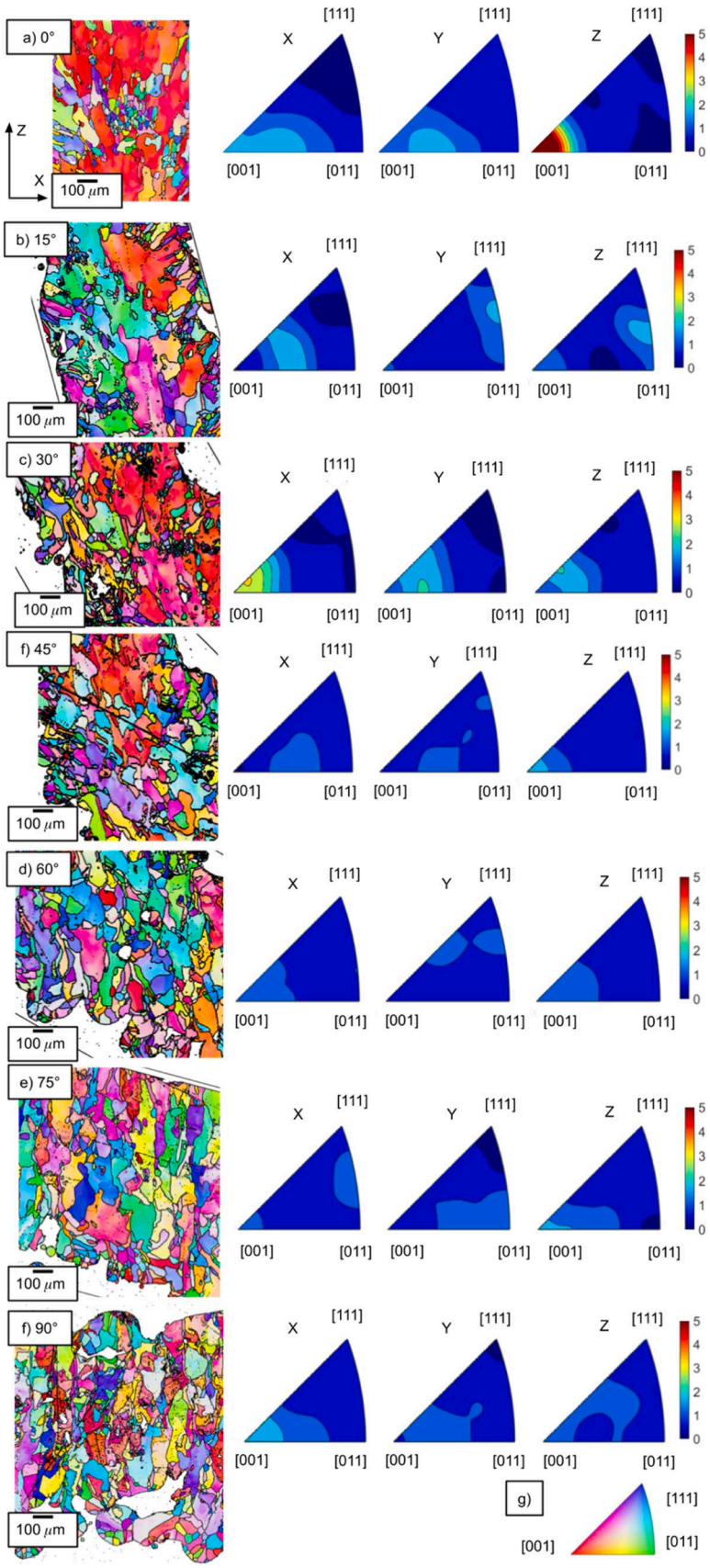

Fig. 3. EBSD data of 0° (a), 15° (b), 30° (c), 45° (d), 60° (e), 75° (f) and 90° (g). Maps of the XZ plane with grain orientation in the XY plane demonstrate a strong ⟨001⟩ texture in the 0° sample, with weak texture in the other samples.

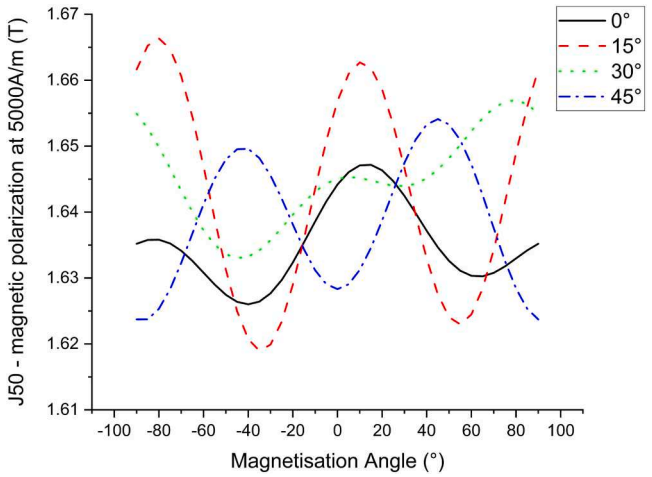

Fig. 4. Calculated changes in J_{50} (magnetic polarisation at 5000 A/m) with magnetisation angle (angle from the long edge of the sample) using EBSD data, demonstrating a small change of less than 3 % between all samples and orientations.

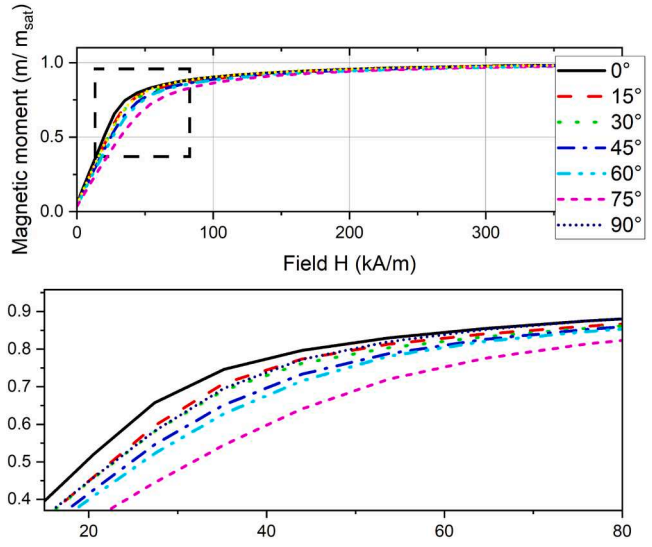

Fig. 5. First quadrant of the MH loop for as-built samples with varying build angle, 0 - 90°, demonstrating a reducing magnetic performance from 0° to 75°, with the 90° sample being an anomaly. Decreasing performance is indicated by a lower magnetisation at the knee point, and a reduced gradient before the knee point.

of the angled samples having a lower density. There does not appear to be a trend as the 15° and 60° samples have >99.5 % density, whereas some of the other samples have lower density. This highlights the need for either more detailed parameter optimisation based on build angle in thin-walled samples, or in-situ process control to allow fully dense samples at any build angle.

EBSD was captured for the XZ plane for all samples between 0 - 90° The EBSD maps were used to plot orientations in the XY plane to confirm if the ⟨001⟩ texture remained with the machine co-ordinate system. EBSD maps for all samples are shown in Fig. 3, demonstrating that the ⟨001⟩ texture remained for the 0° sample with a measure of at least 5 multiples of uniform density (MUD). The other samples all exhibited a weak crystallographic texture with no apparent alignment to the machine coordinate system. The strength of the texture varied between samples, with all samples showing less than 2 multiple of uniform density (MUD), except the 0° and 30° sample. The 30° sample appears to

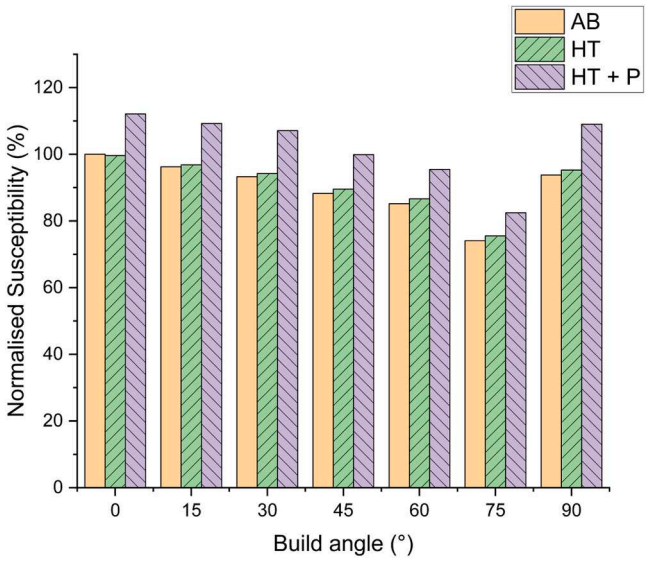

Fig. 6. Normalised susceptibility of as-built (AB), heat treated – 1hr @ 1150 °C (HT), and heat treated with polishing (HT + P), demonstrating a small increase in susceptibility with heat treatment and a large increase with polishing. There is also a decrease in performance with increasing build angle away from vertical (0°). Results are normalised to the 0° as-built sample.

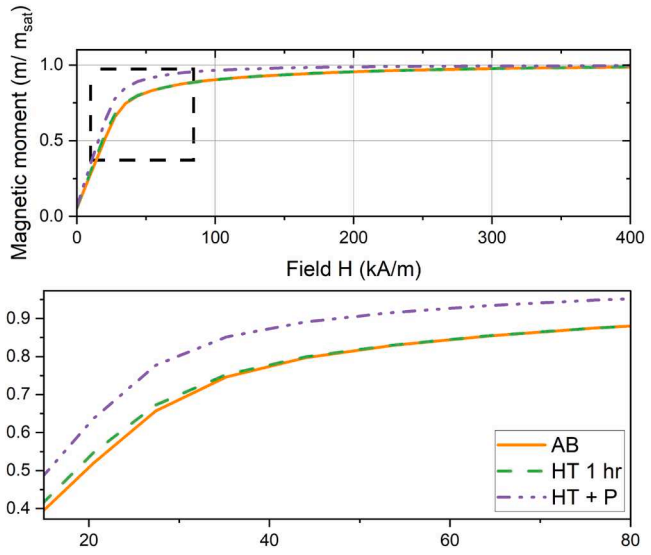

Fig. 7. First quadrant of the MH loop for the as-built, heat treated, and heat treated + polishing samples all built at an angle of 0°, showing that heat treatment has a small positive effect but polishing gives a large improvement with a higher susceptibility and saturation knee point.

have a small texture close to ⟨100⟩, but much weaker than the 0° sample. Hence these results confirm that there is no ⟨100⟩ texture along the build direction for this sample geometry, when the samples move away from vertical (0°).

With the EBSD data it is possible to estimate how the average magnetocrystalline anisotropy energy (E_a) will change when the samples are magnetised at different angles [27]. From this it is possible to calculate the magnetic polarisation J_{50} (at a field, H, of 5000 A/m), shown in Fig. 4. This demonstrates a small range of magnetic polarisations, which varies by only 3 % through all samples and magnetisation angles, hence from EBSD data we can predict little difference in magnetic performance between samples built at different angles.

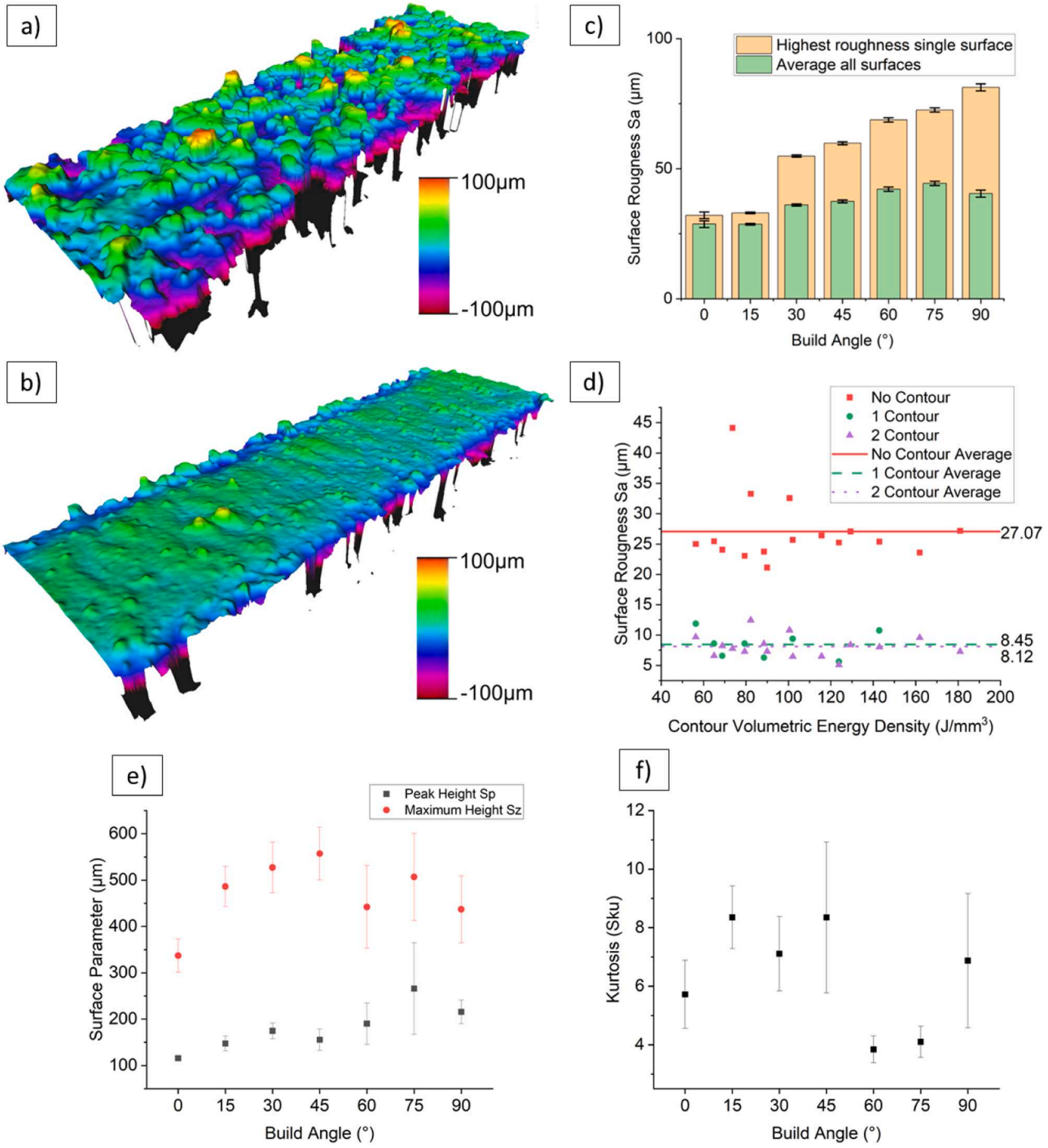

Fig. 8. Surface roughness study showing a sample without contours (a), a sample with 2 contours (b), surface roughness vs build angle (c) which demonstrates an increasing roughness with build angle for the as-built samples, and surface roughness vs contour volumetric energy density (d) which demonstrates a significant improvement in surface roughness with contouring but little difference between 1 or 2 contours.

3.2. VSM measurements

MH loops were measured using VSM by magnetising the sample along its long edge. All samples had the same geometry and are single phase with the same material composition, therefore magnetic moments were plotted normalised to the magnetic saturation (M_{sat}) allowing a more accurate comparison between the data and avoiding shape corrections necessary when using VSM [34]. Fig. 5 shows the first quadrant of the MH loop for all samples 0 - 90°, with the rest of the MH loop excluded for clarity. When investigating the knee point, there is a clear trend of decreasing performance with increasing build angle from sample 0° through to sample 75°, with the 90° sample being an anomaly to this pattern. This performance decrease is demonstrated by a lower magnetisation at a given field, hence a lower susceptibility (X_m), and a higher field required to saturate.

Observations from the EBSD data show that the samples had a weak crystallographic texture therefore are not able to explain the differences in the magnetic properties, supported by the calculations of J_{50} in the previous section. With crystallographic texture not responsible for the change in properties, other factors which could impact the magnetic

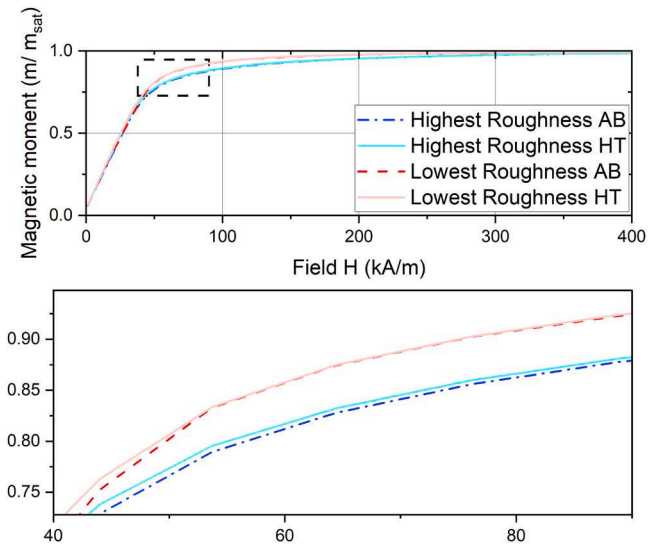

Fig. 9. First quadrant of MH loop demonstrating an improved magnetic performance with a lower roughness in both the as-built and heat treated states. Heat treatment also has a small positive effect on the magnetic performance. The highest and lowest roughness of the samples was 44 μm and 5 μm respectively.

properties were investigated such as residual stress, grain size, and surface roughness.

To reduce residual stress and aim to increase the grain size and susceptibility, a heat treatment (HT) can be used. Annealing at 1150 °C for 1 hr has been shown to have a large positive effect on the permeability and hence susceptibility whilst increasing grain size [6,22] and therefore was used in this study. Fig. 6 demonstrates that the HT has a negligible positive increase of around 1 % in contrast to the other published studies which show order of magnitude improvements. Following HT, to investigate whether surface roughness may have a significant impact on performance, all samples were ground and polished to a surface finish (S_a) of 2 μm before re-testing. Results shown in Fig. 6 demonstrate an increase in normalised susceptibility of at least 10 % for all samples with polishing. Fig. 7 shows the first quadrant of the MH loop for the 0° sample in the as-built, heat treated, and polished with heat treatment condition.

3.3. Surface roughness improvements

As polishing showed a significant increase in susceptibility, further investigation into the as-built surface roughness was undertaken. Surface roughness (S_a) measurements from the as-built 0 - 90° samples show an increasing surface roughness with build angle (Fig. 8c) from 31 μm at 0° to 136 μm at 90° To test if improving the surface finish in the as-built condition improved magnetic properties, samples were manufactured with a build angle of 0°, with contours at a range of volumetric energy densities (VED) ranging from 50 - 180 J/mm^3 with either 0, 1, or 2 contours. By introducing contours, the average surface roughness can be reduced from 27 μm with no contours, to 8 μm with one or two contours (Fig. 8d), giving a visibly improved surface roughness, which is even more evident from optical 3D surface imaging (Fig. 8a/b). Little difference was observed in the surface roughness by varying the VED used for the contours.

Other surface roughness measurements were investigated, with the maximum peak height (S_p) demonstrating a statistically significant linear trend with an R^2 value of 0.91, demonstrating that the maximum peak height increases with build angle, similar to the surface roughness (S_a). The maximum height (S_z) showed no statistically significant linear trend with an R^2 value of 0.27, though it is worth noting the large errors on this measurement especially at 60° build angle and above. The Kurtosis (Sku) also demonstrated no statistically significant linear trend with an R^2 value of 0.50.

Magnetic characterisation was completed for the samples with the highest and lowest surface roughness, of 44 μm and 5 μm respectively. These samples were tested in both the as-built and heat treated condition and the first quadrant of the MH loop is shown in Fig. 9. The results show a clear improvement of magnetic properties with a lower surface roughness, demonstrating a higher susceptibility, higher knee point, and lower field for saturation. Again heat treatment had a small positive impact, but this was small in comparison to the improvement gained with a lower surface roughness.

3.4. Heat treatment improvements

By utilising the heat treatment demonstrated by Garibaldi et al. [22] of 1150 °C for 1 hr, followed by furnace cooling, this study has shown a limited improvement in magnetic properties. Garibaldi et al. demonstrated the recrystallization and grain growth had occurred during this time window. The lack of improvement of magnetic properties suggest that grain growth had not occurred during the heat treatment of the samples in this study. To investigate this, EBSD was carried out for the heat treated samples (1 hr) and the microstructure compared to the as-built samples, for all angles. Fig. 10d shows that for all the samples, the weighted average grain size reduced with the 1 hr heat treatment, demonstrating that partial recrystallisation had occurred but that there had not been sufficient time for grain growth.

To investigate when grain growth would occur in these samples, several samples were built at 0° and heat treated for 1 hr, 3 hrs, 9 hrs, and 30 hrs. Fig. 10e shows that grain growth is still happening up to 30 hrs, where grains of 1 - 2 mm were found in the sample (Fig. 10b). At 30 hrs significant grain growth has occurred and the magnetic properties of the sample were characterised, as shown in Fig. 10c. Interestingly, the magnetic properties of the 30 hrs sample performed below that of the as-built sample demonstrating a lower normalised susceptibility of 92 % (compared to as-built sample). There are multiple factors that could be impacting this, firstly a large amount of porosity was found in the sample during optical microscopy after the heat treatment. Secondly, as the grains are now very large in relation to the sample, the texture of a small number of grains could have a significant impact on the magnetic properties. As shown in Fig. 10b, the texture of the 30 hrs sample is much closer to the ⟨111⟩ direction, which is the hard axis of magnetisation of the material. The last explanation could be due to oxidisation changing the phase from Fe-6.5wt %Si to an iron oxide, with significantly poorer magnetic properties. The heat treatment was supposed to take place under argon; however, an oxide layer was found on the samples during EBSD. Oxygen may have entered into the furnace chamber whilst removing samples with a shorter heat treatment duration.

4. Discussion

This study has shown that for thin-walled samples of high silicon electrical steel, Fe-6.5wt %Si, the crystallographic texture does not cause a significant difference in magnetic performance, contrary to the assumptions of multiple published works. EBSD data has shown that the crystallographic texture does not persist with build angle, and the high silicon content already reduces the magnetocrystalline anisotropy making grain orientation less important. In this study, the performance of thin-walled samples is limited mainly by surface roughness, possibly due to a larger surface to volume ratio inherent in thin-walled samples.

This study highlights the need for different parameters when building parts at different angles, which could be achieved either by a suite of parameters selectively chosen based upon local geometry, or in-situ control algorithms to ensure high density and consistent microstructure. The reduction in density of samples, such as 45°, did not appear to correlate with the decrease in magnetic properties, especially as the

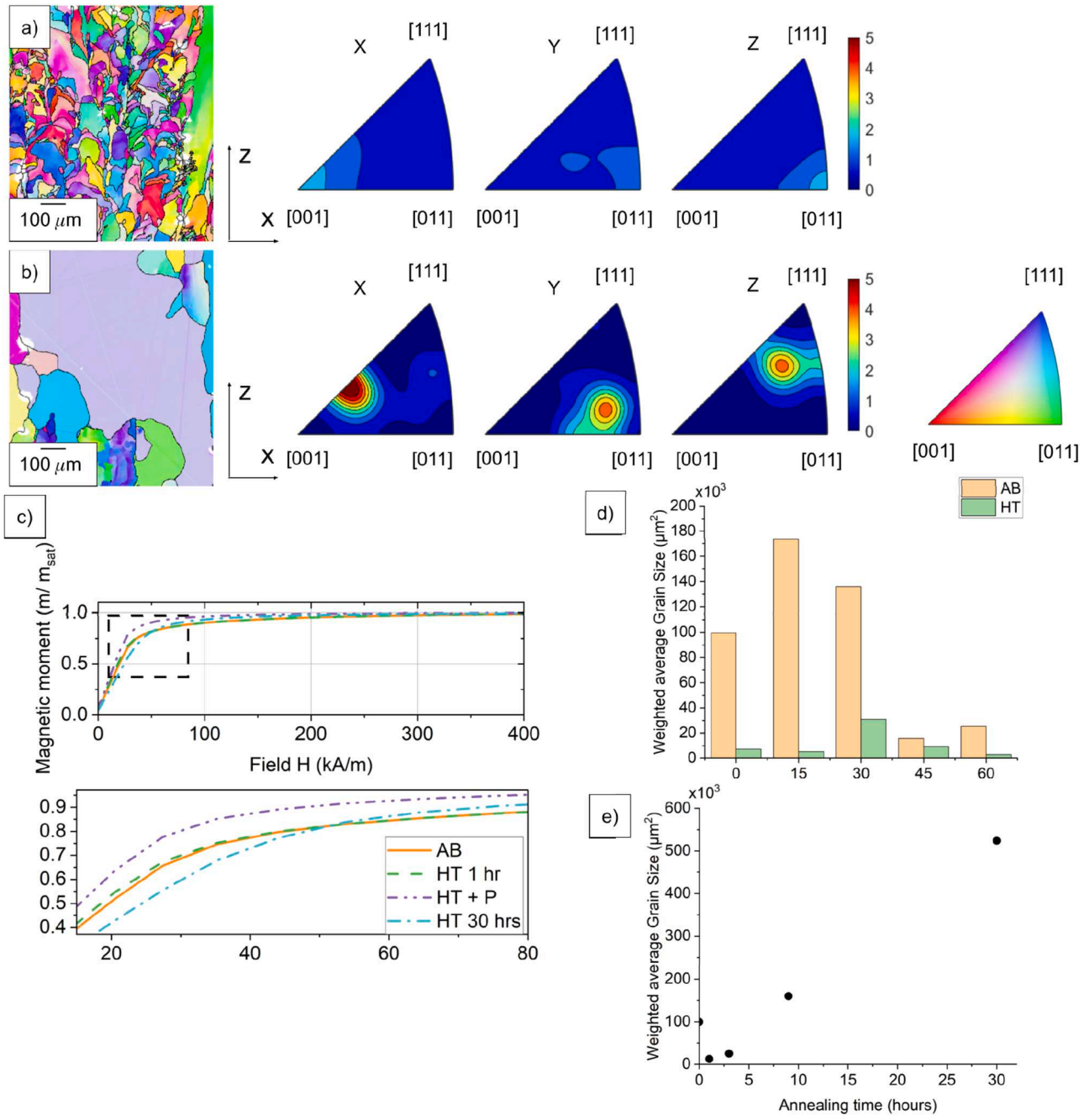

Fig. 10. EBSD data of as-built (a) and heat treated (b) samples with a build angle of 0°, showing partial recrystallisation after heat treatment for 1 h. Magnetic performance of the 30 hr sample dropped in comparison to the AB and 1 hr heat treated samples (c). Weighted average grain size was shown to reduce with 1 hr heat treatment (d), but increase with time up to 30 hr (e). An upper limit for this grain growth was not found in this study.

sample built at 90° had the lowest density but demonstrated third best performance as judged by the MH loops. However, it is likely that any porosity could act as a pinning site. The porosity was based on micrographs of the cross-section of the samples, however a more accurate value may be obtained by X-ray computed tomography (XCT).

Surface roughness is shown to be dependant on build angle, which has previously been reported in the literature [35]. Improvements to surface roughness in the as-built condition are possible and have shown improvements in magnetic properties, though these still have a reduced performance compared to a post-process polishing operation with a surface roughness of 2 μm. This low roughness value is unlikely to be achievable with L-PBF in the near future, and hence other post-processing operations should be investigated such as chemical polishing or electro-polishing. Soft-magnetic materials are likely to require thin wall structures with internal features, making manual polishing difficult. The impact of surface roughness on the magnetic properties such as susceptibility could be due to the pinning of magnetic domains, which may be caused by factors such as excessive roughness or surface features such as partially melted powder particles and spatter.

For soft-magnetic materials, increased pinning of magnetic domains causes a decrease in susceptibility, however for hard-magnetic materials the increased pinning caused by the rough surfaces will increase the coercive force and provide an improvement, as they would be harder to de-magnetise [36].

During this study, the heat treatment as specified by Garibaldi et al. [22] did not cause full recrystallisation and grain growth. The samples in

this study had a small cross-sectional area of 1 mm^2, compared to the larger samples >15 mm^2 for Garibaldi et al. The reduction in cross-sectional area has also reduced the hatch length during the build, which has been positively correlated with residual stress in L-PBF [37], therefore shorter hatches would reduce the residual stress. Higher residual stress is known to lower the temperature of recrystallisation as the sample would have more internal energy and a larger driving factor for nucleation of new grains [38]. The short duration of 1 hr may provide enough time in a larger bulk sample but for thin-walled samples in this study, it proved insufficient and a time of 3 hrs was required for some grain growth, and even after 9 hrs further grain growth was shown. Therefore, in the AM of soft-magnetic components which are likely to require thin wall structures to reduce eddy currents, optimum heat treatment time may be related to component geometry. Hence, investigation will be required on a case-by-case basis, to reduce the heat treatment time to the minimum required for recrystallisation and the desired level of grain growth and magnetic properties whilst remaining economical.

In this study the increased grain growth did not show improved magnetic properties. However, this is more likely due to other factors apparent with the 30 hrs heat treated sample, such as oxidisation, increased porosity, and change of crystallographic texture towards the harder ⟨111⟩ direction.

Magnetic testing during this study was conducted by using VSM on cuboidal samples. VSM testing does not have a flux closed state and hence the magnetostatic energy would be much higher than the magnetocrystalline anisotropy energy. This means that any shape effects would dominate any measurement of anisotropy if the shape was changed. For this study, all the samples used are cuboids of 6 × 1 × 1 mm, hence should have the same magnetostatic energy. However, these were removed from the baseplate by mechanical force and had the potential to leave the samples with slight differences at one of the ends.

5. Conclusion

In this study, thin-walled samples were manufactured using L-PBF, showing a weak crystallographic texture when samples were not built perpendicular to the build platform. By building samples at incremental angles to the build platform, it was possible to magnetically characterise the samples along orientations within the build chamber, which showed a decreasing performance with angle. This decreasing performance was correlated to an increase in surface roughness, which is well-known to decrease with build angle during AM. The sample built at 90° (parallel to build platform) showed an exception to this rule, likely due to the better surface roughness of the top surface which would have no staircase effect typically present in angled surfaces in AM. Improvements in performance were demonstrated by reduced surface roughness as a result of both improved build parameters and post-process polishing. A heat treatment at 1150 °C for 1 hr was shown to be insufficient to cause grain growth in these samples with a 1 × 1 mm cross-section, and grains were shown to still keep growing even after 9 hrs of heat treatment.

Author contributions

(MATLAB processing of EBSD)

CRediT authorship contribution statement

Alexander D. Goodall: Conceptualization, Data curation, Formal analysis, Investigation, Methodology, Writing – original draft. **Lova Chechik:** Software, Writing – review & editing. **Frances Livera:** Methodology, Data curation. **Iain Todd:** Conceptualization, Data curation, Formal analysis, Methodology, Funding acquisition, Supervision, Visualization, Writing – review & editing.

Declaration of Competing Interest

The authors declare that they have no known competing financial interests or personal relationships that could have appeared to influence the work reported in this paper.

Acknowledgements

We wish to acknowledge the Henry Royce Institute for Advanced Materials, funded through EPSRC grants EP/R00661X/1, EP/S019367/1, EP/P02470X/1 and EP/P025285/1, for access to the AconityMINI at The University of Sheffield.

References

[1] B. Zhang, N.E. Fenineche, L. Zhu, H. Liao, C. Coddet, Studies of magnetic properties of permalloy (Fe–30%Ni) prepared by SLM technology, J. Magn. Magn. Mater. 324 (2012) 495–500, https://doi.org/10.1016/j.jmmm.2011.08.030.
[2] T. Pham, P. Kwon, S. Foster, Additive manufacturing and topology optimization of magnetic materials for electrical machines—a review, Energies 14 (2021) 283, https://doi.org/10.3390/en14020283.
[3] T.N. Lamichhane, L. Sethuraman, A. Dalagan, H. Wang, J. Keller, M. P. Paranthaman, Additive manufacturing of soft magnets for electrical machines—A review, Mater. Today Phys. 15 (2020), 100255, https://doi.org/10.1016/j.mtphys.2020.100255.
[4] E.A. Périgo, J. Jacimovic, F. García Ferré, L.M Scherf, Additive manufacturing of magnetic materials, Addit. Manuf. 30 (2019), https://doi.org/10.1016/j.addma.2019.100870.
[5] M. Garibaldi, Laser additive manufacturing of soft magnetic cores for rotating electrical machinery, Mater. Develop. Part Design (2018) 262.
[6] D. Goll, D. Schuller, G. Martinek, T. Kunert, J. Schurr, C. Sinz, et al., Additive manufacturing of soft magnetic materials and components, Addit. Manuf. 27 (2019) 428–439, https://doi.org/10.1016/j.addma.2019.02.021.
[7] A. Plotkowski, J. Pries, F. List, P. Nandwana, B. Stump, K. Carver, et al., Influence of scan pattern and geometry on the microstructure and soft-magnetic performance of additively manufactured Fe-Si, Addit. Manuf. 29 (2019), 100781, https://doi.org/10.1016/j.addma.2019.100781.
[8] A.B. Kustas, D.F. Susan, K.L. Johnson, S.R. Whetten, M.A. Rodriguez, D.J. Dagel, et al., Characterization of the Fe-Co-1.5V soft ferromagnetic alloy processed by Laser Engineered Net Shaping (LENS), Addit. Manuf. 21 (2018) 41–52, https://doi.org/10.1016/j.addma.2018.02.006.
[9] T.F. Babuska, M.A. Wilson, K.L. Johnson, S.R. Whetten, J.F. Curry, J.M. Rodelas, et al., Achieving high strength and ductility in traditionally brittle soft magnetic intermetallics via additive manufacturing, Acta Mater. 180 (2019) 149–157, https://doi.org/10.1016/j.actamat.2019.08.044.
[10] T. Riipinen, S. Metsä-Kortelainen, T. Lindroos, J. Keränen, A. Manninen, J. Pippuri-Mäkeläinen, Properties of soft magnetic Fe-Co-V alloy produced by laser powder bed fusion, Rapid Prototyp. J. 25 (2019) 699–707, https://doi.org/10.1108/RPJ-06-2018-0136.
[11] A.K. Mazeeva, M.V. Staritsyn, V.V. Bobyr, S.A. Manninen, P.A. Kuznetsov, V. N. Klimov, Magnetic properties of Fe–Ni permalloy produced by selective laser melting, J. Alloys Compd. 814 (2020), 152315, https://doi.org/10.1016/j.jallcom.2019.152315.
[12] B. Li, W. Fu, H. Xu, B. Qian, F. Xuan, Additively manufactured Ni-15Fe-5Mo Permalloy via selective laser melting and subsequent annealing for magnetic-shielding structures: process, micro-structural and soft-magnetic characteristics, J. Magn. Magn. Mater. 494 (2020), 165754, https://doi.org/10.1016/j.jmmm.2019.165754.
[13] H. Schönrath, M. Spasova, S.O. Kilian, R. Meckenstock, G. Witt, J.T. Sehrt, et al., Additive manufacturing of soft magnetic permalloy from Fe and Ni powders: control of magnetic anisotropy, J. Magn. Magn. Mater. 478 (2019) 274–278, https://doi.org/10.1016/j.jmmm.2018.11.084.
[14] A. Plotkowski, K. Carver, F. List, J. Pries, Z. Li, A.M. Rossy, et al., Design and performance of an additively manufactured high-Si transformer core, Mater Des. 194 (2020), 108894, https://doi.org/10.1016/j.matdes.2020.108894.
[15] H. Tiismus, A. Kallaste, A. Belahcen, A. Rassõlkin, T. Vaimann, P Shams Ghahfarokhi, Additive manufacturing and performance of E-type transformer core, Energies 14 (2021) 3278, https://doi.org/10.3390/en14113278.
[16] L. Gargalis, V. Madonna, P. Giangrande, R. Rocca, M. Hardy, I. Ashcroft, et al., Additive manufacturing and testing of a soft magnetic rotor for a switched reluctance motor, IEEE Access 8 (2020) 206982–206991, https://doi.org/10.1109/ACCESS.2020.3037190.
[17] H. Tiismus, A. Kallaste, A. Belahcen, M. Tarraste, T. Vaimann, A. Rassõlkin, et al., AC magnetic loss reduction of SLM Processed Fe-Si for additive manufacturing of electrical machines, Energies 14 (2021) 1241, https://doi.org/10.3390/en14051241.
[18] M. Garibaldi, I. Ashcroft, N. Hillier, S.A.C. Harmon, R. Hague, Relationship between laser energy input, microstructures and magnetic properties of selective laser melted Fe-6.9%wt Si soft magnets, Mater. Charact. 143 (2018) 144–151, https://doi.org/10.1016/j.matchar.2018.01.016.

[19] BSI. BS60404-6-2018 Methods of measurement of the magnetic properties of magnetically soft metallic and powder materials at frequencies in the range 20Hz to 100kHz by the use of ring specimens 2018.
[20] L. Chechik, K.A. Christofidou, J.F.S. Markanday, A.D. Goodall, J.R. Miller, G. West, et al., Hardness variation in inconel 718 produced by laser directed energy deposition, Materialia 26 (2022), 101643, https://doi.org/10.1016/j.mtla.2022.101643.
[21] G. Stornelli, A. Faba, A. Schino, P. Folgarait, M.R. Ridolfi, E. Cardelli, et al., Properties of additively manufactured electric steel powder cores with increased Si content, Materials (Basel) 14 (2021) 1489, https://doi.org/10.3390/ma14061489.
[22] M. Garibaldi, I. Ashcroft, J.N. Lemke, M. Simonelli, R. Hague, Effect of annealing on the microstructure and magnetic properties of soft magnetic Fe-Si produced via laser additive manufacturing, Scr Mater. 142 (2018) 121–125, https://doi.org/10.1016/j.scriptamat.2017.08.042.
[23] N. Urban, J. Detrois, J. Franke, Correlation between residual stress, building angle and illumination parameters of additive manufactured FeSi6.5 and mechanical and magnetic properties, in: Proc. 2020 10th Int. Electr. Drives Prod. Conf. EDPC, 2020, pp. 1–7, https://doi.org/10.1109/EDPC51184.2020.9388179.
[24] H.J. Williams, Magnetic properties of single crystals of silicon iron, Phys Rev 52 (1937) 747–751, https://doi.org/10.1103/PhysRev.52.747.
[25] V.M. Paltanea, G. Paltanea, H. Gavrila, L. Dumitru, Experimental analysis of magnetic anisotropy in silicon iron steels using the single strip tester, in: Proc. 2015 9th Int. Symp. Adv. Top. Electr. Eng. ATEE, IEEE, Bucharest, Romania, 2015, pp. 456–459, https://doi.org/10.1109/ATEE.2015.7133857.
[26] T. Yonamine, F.J.G. Landgraf, Correlation between magnetic properties and crystallographic texture of silicon steel, J. Magn. Magn. Mater. 272 (276) (2004) E565–E566, https://doi.org/10.1016/j.jmmm.2003.12.1220.
[27] Magnetic Anisotropy | MTEX n.d. https://mtex-toolbox.github.io/MagneticAnisotropy.html (accessed November 11, 2022).
[28] W. Wu, H. Cao, H. Ou, Z. Chen, X. Zhang, Z. Luo, et al., Effects of punching process on crystal orientations, magnetic and mechanical properties in non-oriented silicon steel, J. Magn. Magn. Mater. 444 (2017) 211–217, https://doi.org/10.1016/j.jmmm.2017.07.003.
[29] H.J. Bunge, Texture Analysis in Materials Science: Mathematical Methods, Elsevier, 2013.
[30] H. Bunge, Texture and magnetic properties, Textures Microstruct. 11 (1989) 75–91, https://doi.org/10.1155/TSM.11.75.
[31] F. Landgraf, T. Yonamine, R. Takanohashi, Q.F. Silva, J. Tosetti, F. Beneduce, et al., Magnetic properties of silicon steel with as-cast columnar structure, J. Magn. Magn. Mater. 254 (2003) 364–366, https://doi.org/10.1016/S0304-8853(02)00869-7.
[32] R. Roy, M. Ghosh, A. Panda, R. Ghosh, A. Mitra, Development of rapidly solidified 6.5 wt% silicon steel for magnetic applications, Trans. Indian Inst. Met. 63 (2010) 745–750, https://doi.org/10.1007/s12666-010-0114-x.
[33] M. Garibaldi, I. Ashcroft, M. Simonelli, R. Hague, Metallurgy of high-silicon steel parts produced using selective laser melting, Acta Mater. 110 (2016) 207–216, https://doi.org/10.1016/j.actamat.2016.03.037.
[34] C.O. Amorim, F. Mohseni, R.K. Dumas, V.S. Amaral, J.S. Amaral, A geometry-independent moment correction method for the MPMS3 SQUID-based magnetometer, Meas. Sci. Technol. 32 (2021), 105602, https://doi.org/10.1088/1361-6501/ac0d23.
[35] P. Delfs, M. Tows, H.J. Schmid, Optimized build orientation of additive manufactured parts for improved surface quality and build time, Addit. Manuf. 12 (2016) 314–320, https://doi.org/10.1016/j.addma.2016.06.003.
[36] J-HKJ-H Kim, S-CSS-C. Shin, High Coercivity in Co/Pt multilayers, Jpn. J. Appl. Phys. 35 (1996) 342, https://doi.org/10.1143/JJAP.35.342.
[37] P. Mercelis, J. Kruth, Residual stresses in selective laser sintering and selective laser melting, Rapid Prototyp. J. 12 (2006) 254–265, https://doi.org/10.1108/13552540610707013.
[38] Toda Caraballo I., Chao J., Lindgren L.E., Capdevila C. Effect of residual stress on recrystallization behavior of mechanically alloyed steels 2010.